

# Evolutionary Machine Learning of Physics-Based Force Fields in High-Dimensional Parameter-Space - Supporting Information

David van der Spoel<sup>1,\*</sup>      Julián Marrades<sup>1</sup>  
Kristian Kříž<sup>1</sup>      A. Najla Hosseini<sup>1</sup>      Alfred T. Nordman<sup>1</sup>  
João Paulo<sup>2</sup>      Marie-Madeleine Walz<sup>1</sup>  
Paul J. van Maaren<sup>1</sup>      Mohammad M. Ghahremanpour<sup>3,\*</sup>

April 30, 2025

<sup>1</sup>: Department of Cell and Molecular Biology, Uppsala University, Box 596, SE-75124, Uppsala, Sweden email:david.vanderspoel@icm.uu.se

<sup>2</sup>: Department of Chemistry, Universidade Federal de Minas Gerais, Belo Horizonte, MG 31270-901, Brazil

<sup>3</sup>: Chemistry Department, Yale University, 8107, New Haven, 06520, CT, USA, email: m.ghahremanpour@hotmail.com

# Contents

<b>1</b>	<b>Supporting physics</b>	<b>S3</b>
<b>2</b>	<b>Supporting tables</b>	<b>S4</b>
<b>3</b>	<b>Parallel implementation and scaling</b>	<b>S14</b>
3.1	Parallel work flow . . . . .	S14
3.2	Strong scaling . . . . .	S14
3.3	Weak scaling . . . . .	S15

# 1 Supporting physics

The 14-7 potential due to Halgren [5] is given by

$$V_{14-7}(r_{ij}) = \epsilon_{ij} \left( \frac{1 + \delta_{ij}}{\frac{r_{ij}}{\sigma_{ij}} + \delta_{ij}} \right)^7 \left( \frac{1 + \gamma_{ij}}{\left(\frac{r_{ij}}{\sigma_{ij}}\right)^7 + \gamma_{ij}} - 2 \right) \quad (\text{S1})$$

where  $\sigma_{ij}$  is the position of the minimum,  $\epsilon_{ij}$  is the well depth at minimum,  $\gamma_{ij}$  and  $\delta_{ij}$  are dimensionless numbers that were originally shared for all elements. However, in our previous work [11], we treated  $\gamma$  and  $\delta$  as free atom-specific parameters subject to optimization and combination rules. In Table S2,  $\gamma$  and  $\delta$  were treated as free parameters, but for trainings for model E and F in Table 1 of the main text,  $\gamma$  was fixed at 0.12 and  $\delta$  at 0.07 [5]. Although there is no guarantee that these numbers are optimal, it is important to prevent over-fitting in force field training to maintain generality (see Table S2 and discussion about that in the main paper).

The Coulomb interaction can be described using Gaussian shielded charges [14, 6, 4]

$$V_{coul}(r_{ij}) = \frac{q_i q_j \text{erf}(\zeta_{ij} r_{ij})}{4\pi\epsilon_0 r_{ij}}, \quad \zeta_{ij} = \frac{\zeta_i \zeta_j}{\sqrt{\zeta_i^2 + \zeta_j^2}}, \quad (\text{S2})$$

where  $\epsilon_0$  is the permittivity of vacuum,  $q_{i,j}$  are the charges and  $\zeta_{i,j}$  are the charge distribution widths (screening factors). The combination rule follows mathematically from the Coulomb integral of two Gaussian-distributed densities. The ACT also supports Slater-functions [4, 15] but those were not used in this paper.

## 2 Supporting tables

Table S1: Dimers used in evaluation of reproducibility of training algorithms (Table S2). N is the number of conformations for each dimer.

Compound	Compound	N	Data set
hydrogen fluoride	hydrogen fluoride	375	Train
hydrogen-chloride	hydrogen-chloride	328	Train
hydrogen-bromide	hydrogen-bromide	311	Train
hydrogen-iodide	hydrogen-iodide	273	Train
hydrogen-bromide	hydrogen-chloride	158	Test
hydrogen-bromide	hydrogen-fluoride	173	Test
hydrogen-iodide	hydrogen-bromide	163	Test
hydrogen-iodide	hydrogen-chloride	164	Test
hydrogen-iodide	hydrogen-fluoride	166	Test

Table S2: Reproducibility of algorithms for training two Van der Waals potentials combined with (Gaussian) electrostatics, including a virtual site for hydrogen halide dimers (Table S1). The number of parameters for the 12-6 potential was 85, for the 14-7 potential it was 107 since  $\gamma$  and  $\delta$  were trained as well. The training dataset consisted of four homodimers (1287 structures), the test set of 10 heterodimers (824 structures). Root mean square deviation of the total interaction energy is given (kJ/mol) after training on the exchange and dispersion energy components and the sum of electrostatics and induction. Intramolecular interactions were excluded. The number of fitness calculations was the same (44800 per training) for all three algorithms, but scaled linearly with population size.

FF	Population	Dataset	MCMC	GA	HYBRID	
12-6[8]	64	Train	6.9	6.7	6.9	
		Test	7.6	5.2	8.1	
	128	Train	6.9	6.9	6.8	
		Test	7.5	7.4	7.5	
	256	Train	6.9	6.8	7.0	
		Test	7.5	6.7	7.6	
	512	Train	6.9	6.9	6.9	
		Test	7.5	7.6	7.6	
	14-7[5]	64	Train	2.7	3.3	2.9
			Test	11.1	10.4	12.1
128		Train	2.7	3.3	2.8	
		Test	11.1	11.6	11.0	
256		Train	2.7	3.0	2.6	
		Test	11.2	11.0	11.2	
512		Train	2.6	2.9	2.6	
		Test	11.1	3.6	11.4	

Table S3: Dimers used in comparison of efficiency of training algorithms. N is the number of conformations for each dimer.

Compound	Compound	N	Data set
diethylene-glycol	methanol	4	Train
2-propanol	propane-13-diol	1	Train
1-propanol	methanol	32	Train
methanol	methanol	60	Train
2-propanol	propane-12-diol	5	Train
2-propanol	2-propanol	6	Train
1-propanol	ethanol	31	Train
water	water	85	Train
2-propanol	methanol	34	Train
methanol	water	60	Train
1-propanol	propane-12-diol	12	Train
2-propanol	ethanol	33	Train
ethanol	methanol	63	Train
1-propanol	propane-13-diol	4	Train
ethanol	ethanol	61	Train
water	ethanol	60	Train

Table S4: List of compound dimers used in training organic compounds and validation in the condensed phase. Since part of the goal here was to exactly reproduce OPLS2020 [10] energies, all dimers were part of the training set. N is the number of conformations for each dimer.

Compound 1	Compound 2	N
ethane	propane	30
ethanol	ethanol	114
ethanol	water	286
water	water	484
1-propanol	ethanol	60
water	1-propanol	109
water	ethane	59
water	propane	59
water	butane	30
ethanol	ethane	11
ethanol	propane	60
ethanol	butane	60
water	1-butanol	73
1-butanol	ethane	11
1-butanol	ethanol	30
1-propanol	ethane	41
1-propanol	propane	30
butane	ethane	11
butane	ethanol	30
butane	propane	41
butane	butane	76
ethane	ethane	100
propane	ethane	111
propane	propane	111
ethanol	butane	60

Table S5: Atomic parameters for 1-propanol from OPLS2020 [10] and from training using ACT. Charges  $q$  (e), Lennard-Jones parameters  $\sigma$  (nm) and  $\epsilon$  (kJ/mol). The parameters in this table completely describe n-alcohols and n-alkanes in OPLS2020. HC is a hydrogen bound to an aliphatic carbon, H1 is a hydrogen bound to a carbon with one electron-withdrawing group, in this the alcohol oxygen, according to the definitions in GAFF [17] that are adopted to some extent in ACT. Model AT has OPLS2020 atom types and was trained to reproduce OPLS2020 energies, while model BT has ACT (chemistry based, see Methods) atom types and was trained to reproduce SAPT energies.

Atom	Param.	OPLS2020 types			ACT types	
		type	OPLS2020	AT	type	BT
C	$q$	54	-0.12	-0.120147	c3	-0.052165
	$\sigma$		0.355	0.354665		0.33651
	$\epsilon$		0.276144	0.280301		0.77848
C	$q$	57	-0.18	-0.17988	c3	-0.0143792
	$\sigma$		0.351	0.350411		see c3 above
	$\epsilon$		0.276144	0.282578		
HC	$q$	60	0.06	0.0600998	hc	0.00624663
	$\sigma$		0.24	0.248409		0.264431
	$\epsilon$		0.108784	0.106474		0.0121607
O	$q$	154	-0.683	-0.682998	o3	-0.640113
	$\sigma$		0.312	0.312184		0.300369
	$\epsilon$		0.71128	0.704655		0.986232
H	$q$	155	0.418	0.418248	ho	0.389719
	$\sigma$		0.0	0.0		0.0964802
	$\epsilon$		0.0	0.0		0.40522
C	$q$	157	0.145	0.144078	c3	0.222554
	$\sigma$		0.350	0.349843		see c3 above
	$\epsilon$		0.276144	0.282107		
H1	$q$	60	0.06	0.0600998	h1	0.00028925
	$\sigma$		0.24	0.248409		0.251253
	$\epsilon$		0.108784	0.106474		0.0873522

Table S6: Atomic parameters for a 4-point water model from TIP4P [9] and from trainings using ACT. Charges  $q$  (e), Lennard-Jones paramters  $\sigma$  (nm),  $\epsilon$  (kJ/mol) and distance of virtual site from oxygen (nm). Model AT has OPLS2020 atom types and was trained to reproduce OPLS2020 energies, while model BT has ACT (chemistry based, see Methods) atom types and was trained to reproduce SAPT energies.

Atom Param.		OPLS2020 types			ACT	
		type	OPLS2020	AT	type	BT
O	q	113	0	-0.0115616	ow	0.0140541
	$\sigma$		0.315365	0.315292		0.305059
	$\epsilon$		0.648520	0.65046		0.905321
H	q	114	0.52	0.520105	hw	0.549881
M	q	115	-1.04	-1.02865	v3bw	-1.11382
	dOM		0.015	0.015192		0.02435091

Table S7: Root mean square deviation (kJ/mol) in energy components for different force fields compared to the SAPT reference. A total of 2114 dimers was included, see Table S4.

Model	Exchange	Dispersion	Electrostatics	Induction	Total
OPLS2020	8.2	2.4	3.7	2.7	2.1
AT	8.2	2.4	3.7	2.7	2.1
AC	8.2	2.4	3.7	2.7	2.1
BT	8.7	2.3	4.3	2.7	1.2
BC	4.3	0.9	3.3	2.7	5.0
C	12.5	3.0	6.1	4.6	2.0
D	13.2	2.8	5.9	4.6	0.8
E	10.9	1.6	3.4	4.6	2.2
F	8.1	1.6	4.4	2.7	1.0

Table S8: Density (g/L, with standard error due to Hess [7]) for ethanol-water mixtures from experiment and molecular dynamics simulations. For the OPLS2020 FF, simulations were performed using GROMACS [12], the ACT-derived models were simulated using OpenMM [2]. The box sizes used here are identical to earlier work by Wensink *et al.* [18]. Except where otherwise mentioned (Table S10), simulations were performed at a temperature of 298.15 K and a pressure of 1 bar. Bond-lengths were constrained to their equilibrium value. Simulation lengths were 1000 ps using a time step of 1 fs. The particle-mesh Ewald method [1, 3] was used to treat long-range electrostatic interactions.

# molecules		Experiment	OPLS	ACT Model		
ethanol	water		2020	C	D	F
391	0	792.7	792.6 (0.7)	779.2 (0.0)	920.1 (0.0)	903.7 (0.0)
352	100	820.4	816.1 (0.8)	808.4 (0.0)	929.6 (0.0)	913.9 (0.0)
313	200	843.8	842.6 (1.0)	832.2 (0.0)	935.4 (0.0)	921.6 (0.0)
274	300	865.5	863.7 (1.3)	850.6 (0.0)	943.8 (0.0)	928.1 (0.0)
235	400	886.4	885.8 (1.3)	870.0 (0.0)	949.8 (0.0)	932.8 (0.0)
196	500	906.1	905.2 (1.8)	889.0 (0.0)	957.2 (0.0)	938.6 (0.0)
156	600	925.7	925.5 (0.7)	909.1 (0.0)	966.5 (0.0)	948.4 (0.0)
117	700	943.8	945.3 (0.9)	929.4 (0.0)	978.0 (0.0)	958.4 (0.0)
78	800	960.7	961.1 (1.7)	949.8 (0.0)	988.0 (0.0)	963.5 (0.0)
39	900	977.1	978.7 (0.9)	973.5 (0.0)	1001.5 (0.0)	975.5 (0.0)
0	1000	997.08	991.8 (1.0)	998.8 (0.0)	1017.8 (0.0)	995.9 (0.0)

Table S9: Density (g/L with standard error due to Hess [7]) for 1-propanol-water mixtures from experiment and molecular dynamics simulations. For the OPLS2020 FF, simulations were performed using GROMACS [12], the ACT-derived models were simulated using OpenMM [2]. The box sizes used here are identical to earlier work by Wensink *et al.* [18]. See Table S8 for simulation details.

# molecules		Experiment	OPLS	ACT Model		
1-propanol	water		2020	C	D	F
300	0	803.73	803.2 (1.4)	794.9 (0.0)	935.5 (0.0)	922.7 (0.0)
270	100	826.70	824.3 (2.8)	817.3 (0.0)	940.3 (0.0)	926.0 (0.0)
240	200	847.53	845.0 (1.5)	837.5 (0.0)	947.2 (0.0)	932.0 (0.0)
210	300	867.93	865.6 (1.4)	855.5 (0.0)	952.7 (0.0)	936.9 (0.0)
180	400	888.37	881.1 (0.8)	875.3 (0.0)	958.4 (0.0)	943.3 (0.0)
150	500	908.77	904.2 (0.9)	893.4 (0.0)	966.5 (0.0)	947.2 (0.0)
120	600	929.60	921.4 (2.0)	913.8 (0.0)	972.9 (0.0)	956.0 (0.0)
90	700	950.30	940.2 (0.9)	932.7 (0.0)	982.3 (0.0)	964.2 (0.0)
60	800	969.63	959.6 (1.0)	954.8 (0.0)	991.9 (0.0)	969.1 (0.0)
30	900	985.07	979.1 (1.4)	975.3 (0.0)	1004.9 (0.0)	978.4 (0.0)
0	1000	997.08	991.8 (1.0)	998.8 (0.0)	1017.8 (0.0)	995.9 (0.0)

Table S10: Density (g/L with standard error due to Hess [7]) of alkanes from liquid simulations using the OPLS2020 model [10], simulated using GRO-MACS [12] and models derived in this work, simulated using OpenMM [2]. For simulation details see Table S8.

Compound	N	T (K)	Exper.	OPLS	C	ACT Model	
				2020		D	F
methane	1000	100	438	471.6 (1.7)	459.5 (0.0)	513.1 (0.0)	457.2 (0.0)
ethane	500	150	577	587.6 (1.3)	576.9 (0.0)	658.3 (0.0)	630.2 (0.0)
propane	333	200	620	575.2 (2.4)	609.3 (0.0)	710.3 (0.0)	689.2 (0.0)
butane	250	250	626	622.6 (2.5)	616.8 (0.0)	724.3 (0.0)	701.8 (0.0)
isobutane	250	250	607	626.9 (4.1)	614.6 (0.0)	729.2 (0.0)	705.6 (0.0)
cyclopentane	200	298.15	750	721.4 (0.9)	699.8 (0.0)	845.3 (0.0)	858.7 (0.0)
pentane	200	298.15	621	611.5 (2.7)	605.3 (0.0)	720.6 (0.0)	693.3 (0.0)
neopentane	200	298.15	586	605.6 (3.7)	609.7 (0.0)	737.1 (0.0)	713.2 (0.0)
cyclohexane	166	298.15	773	761.3 (1.4)	760.3 (0.0)	904.9 (0.0)	887.5 (0.0)
hexane	166	298.15	656	643.2 (1.7)	651.3 (0.0)	760.6 (0.0)	732.8 (0.0)
octane	125	298.15	699	700.8 (1.6)	709.3 (0.0)	811.7 (0.0)	780.7 (0.0)
RMSD				23	20	108	87
MSE				-3	-4	51	94

Table S11: Density (g/L) of alkali halides from simulations starting from the crystal state at 298.15 K. The reference data were taken directly from the paper by Walz *et al.* [16]. Those simulations were performed using GROMACS 4.6.7 [13] using self-consistent optimization (SCF) of drude positions at each time step in the simulations. Here, we performed simulations of 500 ps using OpenMM [2] on a NVIDIA GPU with the same integration algorithm. N denotes the number of ion-pairs in the crystal.

Salt	N	Exper.	Walz [16]	This work
LiF	500	2638	2638	2653
LiCl	500	2076	2075	2079
LiBr	500	3465	3466	3467
LiI	500	4069	4070	4050
NaF	500	2803	2803	2825
NaCl	500	2166	2167	2182
NaBr	500	3201	3202	3207
NaI	500	3671	3667	3667
KF	500	2524	2524	2534
KCl	500	1988	1990	2003
KBr	500	2749	2746	2763
KI	500	3125	3124	3137
RbF	500	3844	3844	3878
RbCl	500	2820	2819	2837
RbBr	500	3360	3361	3369
RbI	500	3565	3558	3558
CsF	500	4638	4640	4668
CsCl	512	3990	3987	4023
CsBr	512	4460	4461	4464
CsI	512	4526	4530	4549

### 3 Parallel implementation and scaling

#### 3.1 Parallel work flow

Fig. S1 shows the parallelization scheme for the training code in the ACT.

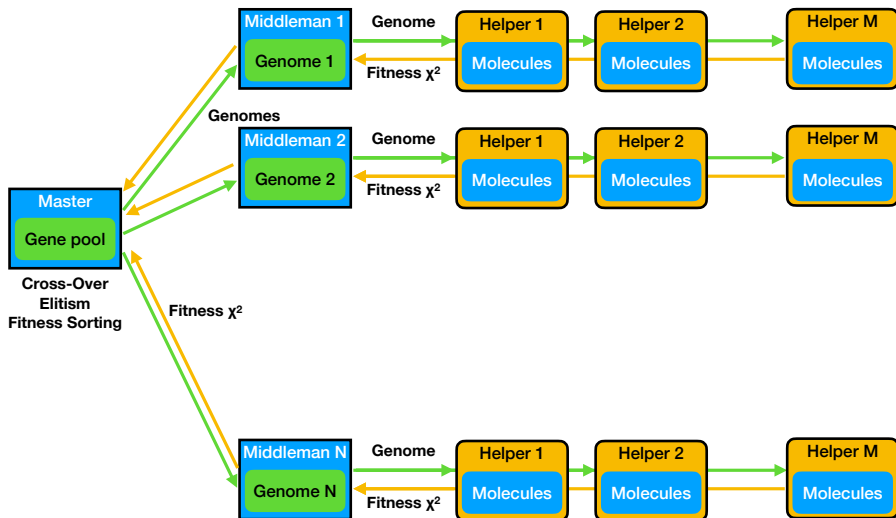


Figure S1: **Schematic showing the parallelization and flow of information in force field optimization in the ACT.** The master process hands out genomes from the gene pool to all the middlemen. Those in turn perform fitness calculations and local optimization using Monte Carlo. If needed, helper processes can be used to speed up the calculation. The communication between middleman and helper is local only to reduce overhead. The master process receives the fitness and the mutated genomes from the middleman, sorts them and performs cross-over to produce offspring.

#### 3.2 Strong scaling

Strong scaling is evaluated by increasing the number of cores for a given problem and can be computed as

$$S_s = 100 \times \frac{128t_{128}}{nt_n} \quad (\text{S3})$$

with  $n$  representing the number of cores, 128 being the reference, and  $t_n$  the run time. Fig. S1 depicts the parallelization scheme used in the ACT, consisting of three layers: a master process controlling the middlemen which act as individuals in the population and helpers for the middlemen. When the MCMC algorithm is used there is no communication between middlemen. However, with increasing number of cores, the compounds are divided over helper nodes necessitating local communication. Doubling the number of cores for MCMC improves the throughput ( $S_s > 1$ , Fig. 2B in main article) which is typically due to better usage of cache memory. Until three helpers per middleman (512 cores) scaling  $S_s$  remains close to one. For the other two methods, global communication is involved at each generation in the genetic algorithm and performance decreases quite rapidly. It could be expected that the performance of the HYBRID algorithm would be in-between the other two since there is much less communication than in the GA algorithm. Perhaps the very small size of the training set exaggerates the cost of communication. Running a short evaluation like this before full-scale force field training may aid in optimizing resource usage.

### 3.3 Weak scaling

Weak scaling, that is the change of CPU time with increasing calculation load, was evaluated for the training of an alcohol force field (Table S12). For both HYBRID and MCMC increasing the number of fitness evaluations by a factor of four reduces the efficiency by 5% only. For the pure GA algorithm there is more communication, and performances falls by 11% (Table S12).

Table S12: Performance statistics for different algorithms. Timing and weak scaling (compute effort proportional to number of cores) are given as well as the final fitness  $\chi^2$  (lower is better). Benchmark system is given in Table S4, there were 41 parameters to train. Training was set up such that all algorithms did the same amount of energy calculations. Scaling is defined in the main text. Calculations were run on a Cray where each node had two AMD EPYC 7742 64-core processors.

Algorithm	Population	#Generations	#MCMC	Time (s)	$S$ (%)	$\chi^2$
GA	128	32800	-	3489	100	38.8
	256	32800	-	3635	96	29.5
	384	32800	-	3761	93	32.8
	512	32800	-	3925	89	37.8
MCMC	128	1	800	3376	100	29.5
	256	1	800	3435	98	29.4
	384	1	800	3516	96	29.5
	512	1	800	3566	95	29.5
HYBRID	128	20	40	3402	100	29.5
	256	20	40	3434	99	29.4
	384	20	40	3586	95	29.5
	512	20	40	3562	96	29.4

## References

- [1] T Darden, D York, and L Pedersen. Particle mesh Ewald: An N-log(N) method for Ewald sums in large systems. *J. Chem. Phys.*, 98:10089–10092, 1993.
- [2] Peter Eastman, Raimondas Galvelis, Raúl P. Peláez, Charles R. A. Abreu, Stephen E. Farr, Emilio Gallicchio, Anton Gorenko, Michael M. Henry, Frank Hu, Jing Huang, Andreas Krämer, Julien Michel, Joshua A. Mitchell, Vijay S. Pande, João PGLM Rodrigues, Jaime Rodriguez-Guerra, Andrew C. Simmonett, Sukrit Singh, Jason Swails, Philip Turner, Yuanqing Wang, Ivy Zhang, John D. Chodera, Gianni De Fabritiis, and Thomas E. Markland. Openmm 8: Molecular dynamics simulation with machine learning potentials. *J. Phys. Chem. B.*, 128:109–116, 2024.
- [3] U Essmann, L Perera, M L Berkowitz, T Darden, H Lee, and L G Pedersen. A smooth particle mesh Ewald method. *J. Chem. Phys.*, 103:8577–8592, 1995.
- [4] Mohammad Mehdi Ghahremanpour, Paul J. van Maaren, Carl Caleman, Geoffrey R. Hutchison, and David van der Spoel. Polarizable drude model with s-type gaussian or slater charge density for general molecular mechanics force fields. *J. Chem. Theory Comput.*, 14:5553–5566, 2018.
- [5] Thomas A Halgren. The representation of van der Waals (vdW) interactions in molecular mechanics force fields: potential form, combination rules, and vdW parameters. *J. Amer. Chem. Soc.*, 114:7827–7843, 1992.
- [6] G G Hall and K Tsujinaga. The molecular electrostatic potential of some simple molecules. *Theor. Chim. Acta.*, 69:425–436, 1986.
- [7] B Hess. Determining the shear viscosity of model liquids from molecular simulation. *J. Chem. Phys.*, 116:209–217, 2002.
- [8] J E Jones. On the determination of molecular fields. -II. From the equation of state of a gas. *Proc. Royal Soc. Lond. Ser. A*, 106:463–477, 1924.

- [9] W L Jorgensen, J Chandrasekhar, J D Madura, R W Impey, and M L Klein. Comparison of simple potential functions for simulating liquid water. *J. Chem. Phys.*, 79:926–935, 1983.
- [10] William L. Jorgensen, Mohammad M. Ghahremanpour, Anastasia Saar, and Julian Tirado-Rives. OPLS/2020 force field for unsaturated hydrocarbons, alcohols, and ethers. *J. Phys. Chem. B.*, 128:250–262, 2023.
- [11] Kristian Kríž, Paul J. van Maaren, and David van der Spoel. Impact of combination rules, level of theory and potential function on the modelling of gas and condensed phase properties of noble gases. *J. Chem. Theory Comput.*, 20:2362–2376, 2024.
- [12] Szilárd Páll, Mark James Abraham, Carsten Kutzner, Berk Hess, and Erik Lindahl. Tackling exascale software challenges in molecular dynamics simulations with gromacs. *Lect. Notes Comput. Sci.*, 8759:3–27, 2015.
- [13] Sander Pronk, Szilárd Páll, Roland Schulz, Per Larsson, Pär Bjelkmar, Rossen Apostolov, Michael R Shirts, Jeremy C Smith, Peter M Kasson, David van der Spoel, Berk Hess, and Erik Lindahl. GROMACS 4.5: a high-throughput and highly parallel open source molecular simulation toolkit. *Bioinformatics*, 29:845–854, April 2013.
- [14] C M Smith and G G Hall. The approximation of electron densities. *Theor. Chim. Acta.*, 69:63–69, 1986.
- [15] David van der Spoel, Paul J. van Maaren, and Mohammad M. Ghahremanpour. *Alexandria Chemistry Toolkit Reference and User Manual version 1.0*. The Alexandria Chemistry Project, Uppsala, Sweden, 2025.
- [16] Marie Madeleine Walz, Mohammad M. Ghahremanpour, Paul J. van Maaren, and David van der Spoel. Phase-transferable force field for alkali halides. *J. Chem. Theory Comput.*, 14:5933–5948, 2018.
- [17] J Wang, R M Wolf, J W Caldwell, P A Kollman, and D A Case. Development and testing of a general AMBER force field. *J. Comput. Chem.*, 25:1157–1174, 2004.
- [18] E J W Wensink, A C Hoffmann, P J van Maaren, and D van der Spoel. Dynamic properties of water/alcohol mixtures studied by computer simulation. *J. Chem. Phys.*, 119:7308–7317, 2003.